Supplemental Material, Lyle et al "Equatorial Pacific Carbonate cycles, 0-5 Ma: stratigraphy, dissolution, and paleoproductivity"

The supplemental material for this paper consists of data used to correlate 7 equatorial Pacific scientific drill sites (Figure
5 SM-1), develop a common age model, and document mass accumulation rates of CaCO$_3$ and other sediment components estimated by XRF scanning and bulk density.

The supplemental material contains: 1) Splice interval tables for all sites used to create the continuous sedimentary section, plus splice interval tables for the remaining Leg 138 drill sites; 2) site to site depth ties used to create equivalent depth
10 matches among the different sites and with an age model, equivalent ages; 3) Benthic stable isotope records from Site 849 and U1338 and an age model combining a younger section of benthic stable isotope data from ODP Site 849 with an older section from IODP Site U1338; 4) XRF data from IODP Sites U1335, U1337, and U1338 with ages interpolated; 5) Additional XRF data from ODP Site 849; 6) Estimated CaCO$_3$% from GRA density for ODP Sites 848, 850, and 851 and the algorithm used to estimate CaCO$_3$; and, 7) Mass accumulation rate data at 10 kyr intervals for CaCO$_3$ (all sites), opal (Sites
15 849, U1338, U1337), clay (Sites 849, U1338, U1337), and other minor elements (Sites U1337 and U1338).

1 Splice Data for Drill Sites in this paper.

Data needed to splice a continuous sediment section from multiple drill holes and to match stratigraphic intervals in adjacent holes are presented in **Tables SM-1 to SM-7** for ODP Leg 138 sites 848, 849, 850, and 851, as well as for IODP Expedition 320/321 Sites U1335, U1337, and U1338.
20

The tables will be familiar to ODP and IODP users, and are used to splice together sections of sediment core from adjacent holes to make a continuous section over core breaks in adjacent holes and/or avoid disturbed sections near the start and end of recovered sediment cores. Offsets are a linear depth adjustment used to align stratigraphically equivalent intervals in cores from adjacent holes. Original coring depth is referred to as mbsf (meters below sea floor) in ODP sites and as CSF-A (coring
25 depth below sea floor-method A) in IODP sites. The adjusted depth where offsets are added are referred to as mcd (meters composite depth) in ODP sites and CCSF (composite coring depth below sea floor) in IODP. In the supplemental material and all tables, we refer to all coring depths as CSF (all based on method A), and all adjusted depths as CCSF. The interval table at each site lists sedimentary sections that are included in the splice section, while tie tables list where sections in the splice are tied to the top of the next section included in the splice in an adjacent hole.
30

We have redone splices from Leg 138 using Code for Ocean Drilling Data (CODD, Wilkens et al, 2017). The original Leg 138 splices were done before standardization of how splices were reported and were sometimes ambiguous. However, initial splices used Hagelberg et al. (1995) offsets. Checking the splice with CODD was relatively straightforward and we report here tables for Sites 848, 849, 850, and 851 that were rechecked and adjusted. We use the shipboard splice for Site U1335 and the revised Site U1338 splice is that reported in Wilkens et al (2013). The bulk of Site U1337 is from Wilkens et al (2013) but a mismatch in ties was found in the lower Miocene section (core U1337C-20) that has been corrected in the splice reported in **Table SM-6**.

We redid the Site 849 splice using the new XRF scanning data (Section 4.2) as well as the shipboard-collected multisensor track data used by Hagelberg et al. (1995). In the uppermost part of the core, we spliced around one section in the original splice that was sampled to the point that it could not be XRF scanned. The changes from the Hagelberg et al (1995) splice are small, except below 849D-13. By comparison with other cores and the logs, we determined that core 849B-14 should added to the splice and found a tie to 849D-13. Core 849D-14 did not overlap with 849 B-14, and was appended.

We estimated the amount of missing section between cores 849B-14 and 849D-14 by comparing the splice section across the break in the splice to logs taken from 849B. We used the IMPH medium resistivity log since it is less affected by drill hole damage found in the upper part of U849B (Mayer et al., 1992). We downscaled the XRF data to log measurements (15.24 cm between data points) and aligned the compressed $CaCO_3$ splice and the IMPH log data above the splice break. We found that the core data needed to be shifted down by 30 cm to match below the break, i.e., that 30 cm of core was missing between the appended cores. We added 30 cm to the 849 splice depths at the base of 849B-14 where it is appended to 849D-14. These changes alter the lower part of the original Mix et al (1995) isotope splice for Site 849 (**Table SM-14**).

2 Depth Matching Sites 848, 849, 850, and 851 with U1338, U1337, and U1335

All sites in this paper were depth matched using the whole round scan data (GRA density, Magnetic susceptibility, p-wave velocity) collected on board the *JOIDES Resolution* and XRF data where available. CODD software developed by Wilkens et al (2017) was used to make depth ties between spliced sections from each site.

Once spliced sediment columns have been made at each site, the CODD software allows core depths from a drill site to be stretched/squeezed to match physical property records to those from a reference site. The matching assumes that changes in physical properties are chronostratigraphic. Matching independent datum levels from biostratigraphy, paleomagnetic stratigraphy, and stable isotope stratigraphy constrains the matches made between physical properties profiles (Figure SM-2). In the case of equatorial Pacific drillsites, all physical properties variability maps to changes in $CaCO_3$ content.

2

Positions of biostratigraphic datum levels or magnetic reversals are depth marked on the splice records by the CODD software to aid with the hole-to-hole correlations. The ultimate result of the matching is a set of drill sites in a common depth framework. To maximize the likelihood that the matches are chronostratigraphic, Sites 848 and 850 were matched to Site 849, while Sites 851, U1335, and U1337 were matched to Site U1338. Finally, Site 849 was depth matched to Site U1338 in order that an equivalent depth in Site U1338 could be propagated to all sites. Once the common depth framework has been achieved, a common age model can then be imposed on all sites as described in Section 3. Ties between individual sites are listed in **Tables SM-8 to SM-13**.

Site U1338 is the primary base site for depth matching. The depth matching between Site U1338 and Site 849 was particularly important to establish age models from the combined Expedition 320/321 and Leg 138 data sets. We mostly used XRF data and GRA bulk density data to make a match to 347.25 m CCSF in Site 849 and 221.31 m CCSF in U1338, or roughly to an age of 10 Ma (See U1338-849 tie table, **Table SM-10**).

Site 849 is the primary site used to depth match Sites 848 and 850. Matching Site 850 to Site 849 was straightforward because of the similarity in the diatom deposition intervals at both sites. However, Site 851 is strongly similar to Site U1338, at the same latitude, so it was matched directly to Site U1338. Site 848 provided some challenge because of its relatively slow sedimentation rate, but correlations made earlier by Shackleton et al. (1995) as well as the biostratigraphic datum levels assured a reasonable match to Site 849.

3 Common age model for Site 848, 849, 851, U1335, U1337, and U1338.

We have made a new 0-8.2 Ma age model for the eastern equatorial Pacific based on tuned benthic foraminiferal oxygen isotopes. We revised the age model for Site 849 isotope data collected by Mix et al (1995) We redid the Site 849 splice based on GRA and XRF data, and found minor changes except below Site 849D-13H where we added a missing section. We re-spliced the oxygen isotope data based on these new depth parameters (**Table SM-2**). By using the common depth framework between Site 849 and U1338, we could determine that there were missing sections of data at Site 849 between 122.9 to 127.0 m CCSF and 141.0 to 143.3 m CCSF in the Mix et al (1995) data. Fortunately these intervals overlap with the U1338 isotope data. The Site 849 age model was tuned to the Wilkens et al (2017) Ceara Rise benthic foraminiferal isotope stack. We use the Ceara Rise stack rather than the Lisiecki and Raymo (2005) stack because there is a strong precessional beat in the Ceara Rise data that better enables tuning. Wilkens et al (2017) noted that the overall agreement with the LR04 δ^{18}O stack (Lisiecki and Raymo, 2005) is quite good, except around 1.8 Ma and between 4 and 4.5 Ma. The 1.8-1.9 Ma difference perhaps indicates a misalignment when the LR04 switched age models near this point. The interval older than 4 Ma in the LR04 stack has only a small number of data records with low amplitude variability of the oxygen isotope values.

3

The Site 849 data were spliced to the Site U1338 isotope data from Drury et al (2016) from 3.5 Ma to 8.0 Ma. For Site U1338, we used the astrochronology developed by Drury et al. (2018) for Site U1338 between 3.5-8.0 Ma, which revised the benthic stable isotope age model in Drury et al (2016): depth matches between Sites U1337 and U1338 allowed the better astro-magnetochronology from Site U1337 to constrain ages at Site U1338 through the late Miocene (8.0-6.0 Ma), while the remaining 6.0-3.5 Ma interval was astronomically tuned using the benthic $\delta^{18}O$ data (Drury et al, 2017; Drury et al., 2018).

The combined age model uses ages from Site 849 grafted to the Site U1338 age model below 3626 ka (Figure SM-3). The Site 849 isotope record was cut at 100.35 m CCSF in Site 849 (3624.98 ka, 49.025 m CCSF in U1338 equivalent depth) and grafted to the Site U1338 isotope record at 3626.04 ka (49.13 CCSF in U1338) for the combined age model. Site 849 provides the younger section from 0 to 3625 ka and Site U1338 provides the section from 3626 Ka to 8180 ka (**Tables SM-14 to SM-16**).

The site-to-site correlation in the CODD package produces a direct equivalent depth measurement in each of the sites correlated to Site either U1338 or 849. We used the combined Site 849-U1338 age model and the depth matching we made between these two sites and the other sites in the paper to impose an age model by assigning ages to the equivalent depths. Ages are reported to 8180 ka for the estimated $CaCO_3$ from GRA data (Section 5) and the XRF data tables (Section 4).

4 XRF data

XRF scanning data for Sites U1335, U1337, and U1338 are reported here along with calibrations to convert to percentage data. Original XRF scanning data are reported in Lyle et al. (2012) and Shackford et al. (2014). Data are reported in **Tables SM-17 to SM-19.**

4.1 Sites U1335, U1337, and U1338 XRF data and splice, IODP Exp 321:

Sites U1335 and U1338 were XRF scanned along the Wilkens et al (2013) and Site U1337 data are reported along the revised splice (**Table SM-6**). Ages are applied for the 0-8180 ka that lies within the age model for this paper. Data below this interval is still included in the tables and depth ties allow site-to-site correlation below the bottom of the isotope age model.

The spliced data for U1335, U1337, and U1338 were scanned in 2009/2010 using the ODASES Avaatech XRF scanner at the IODP Gulf Coast Repository and the raw and NMS-processed data are available in Lyle et al. (2012) and Shackford et al. (2014). Wilson (2014) and Lyle and Baldauf (2015) contain the calibrated data sets for Site U1337 and Site U1338, respectively.

4

Normalized median-scaled (NMS) data listed in **Tables SM-17 through SM-19** were calculated by the method in Lyle et al (2012) and were then calibrated by correlation to discrete ICP-MS analysis for Al, Ti, Mn, Fe, and Ba, and by shipboard and shore-based $CaCO_3$ analysis for Ca (Lyle and Backman, 2013; Wilson, 2014; Lyle and Baldauf, 2015). For $CaCO_3$, the correction for aluminosilicate Ca is small when the clay fraction is less than 10% as in the equatorial Pacific (Dymond et al, 1976).

Total SiO_2 data were calibrated to opal data adjusted upward for a small clay component, averaging between 5 and 10% of the bulk sediment. There was no ICP-MS data for Si because the acid used in the ICP-MS analysis was Si contaminated. A small addition of Si to account for clay Si was added to the opal totals based on SiO_2/TiO_2 in average upper continental crust (Taylor and McClennon, 1995) and using the calibrated XRF TiO_2 to calculate the addition. We measured opal SiO_2 on a set of discrete samples using the leach procedure of Olivarez-Lyle and Lyle (2002) modified by using a 1M KOH solution rather than a 2M solution. Then we added the clay-bound SiO_2 estimated by the TiO_2 content from the calibrated XRF data to get total SiO_2 for calibration. We used the XRF TiO_2 calibrated by discrete ICP-MS and an upper continental crust SiO_2/TiO_2 ratio of 131.54 (Taylor and McLennan, 1995) to estimate a clay-bound SiO_2 to be added to the measured opal SiO_2 to get total SiO_2. Subsequently, opal SiO_2 was calculated by subtracting the normative clay-bound SiO_2 (using XRF TiO_2) from the calibrated XRF total SiO_2%. The clay-bound SiO_2 correction is small, and does not affect opal trends.

4.2 Site 849 XRF data and splice, ODP Leg 138:

We XRF scanned along the revised splice and offsets in **Table SM-2**. Site 849 XRF data reported here (**Table SM-20**), are from two separate XRF scanning campaigns, in 2013 and 2014. The 2013 scan starts at the sea floor and goes to a depth of 168.67 m CCSF (base of U849B-16X). A second set of XRF data from the Site 849 splice were scanned in October 2014 and joined to the previous XRF data set. The final depth of the U849 XRF data reported here is 286.72 m CCSF, at the base of 849B-27X. Based on the composite age model, the age at the base of the XRF section is 7204 ka.

A problem in scanning older cores is that the cores have shrunk since collection since they have partially dried out. For the Site 849 APC section, the cores tended to shrink as a unit in the section, so the section was displaced ~10 cm from one of the section ends. In the XCB section, which was biscuited, cracks formed uniformly along the section between biscuits, so the measured length remained similar to the original length; the cracks just got larger. Shrinkage was handled in the APC section by measuring the length of the sediment relative to the core tube and assuming the core tube was originally full. XRF depths were then re-expanded by multiplying by the ratio of core tube length/ current sediment length.

We scanned the Site 849 splice at 2 cm spacing with the ODASES Avaatech XRF scanner housed at the IODP Gulf Coast Repository (https://iodp.tamu.edu/labs/xrf/) using 10 kV excitation and 500 mA power for 30 seconds live time. We

collected data for the elements Al, Si, K, Ca, Ti, Mn, Fe, and Ba. We processed the data to NMS values (Lyle et al, 2012) to remove porosity and crack artifacts and to minimize the differential caused by different XRF responses of different elements.

Because the XRF tube was beginning to fail in 2013, we only did a 10 kV scan and not the 50 kV typically used for Ba, and used the Ba L-α fluorescence peak from the 10 kV scan for Ba. The XRF tube failed and was replaced between the 2013 and 2014 campaigns, so that there may be some offset between the two sets of data. Because of the low levels of clays below 125 m, Ti and Al were often below detection limits below 125 m CCSF. Since we did not do additional ICP-MS bulk sediment analyses we calibrated the $CaCO_3$ to shipboard $CaCO_3$ measurements and used discrete opal measured at TAMU in 2013 and 2014 (**Table SM-21**) to calibrate an estimated opal %. Since clay-bound SiO_2 is known to be low (Winckler et al, 2008), we correlated total SiO_2 with measured opal. The linear calibrations to estimate opal and CaCO3% are as follows:

$$Opal \% = 0.765*SiO_2\_NMS -2.293 \hspace{4cm} (1)$$
$$CaCO_3 \% = 0.956*CaCO_3\_NMS +4.83 \hspace{3.5cm} (2)$$

We were also able to crudely calibrate clay by correlating XRF Fe_2O_3 NMS data to dust estimated by [232]Th. We used Winkler et al (2008) [232]Th measure of dust in the upper 400 kyr of Site 849 and typical Th and Fe in upper continental crust (Taylor and McClennan, 1995) to correlate XRF Fe_2O_3 NMS to Th and then used the average upper continental crust to represent the clay fraction. Unfortunately, [232]Th data were only available for the upper 13.65 m. We did not use TiO_2 to estimate clay because TiO_2 was frequently below detection limits in the lower XRF section below 125 m CCSF. Fe and Ti were well correlated in the upper section, suggesting that most of the Fe resides in clays. The calibration equation we used was

$$Clay \% = 2.393*Fe2O3\_NMS +1.25 \hspace{4cm} (3)$$

We were also able to calibrate Ba to the Ma et al (2015) barite data from Site 849. For the most part the trends of data were similar, except in the diatom-rich interval between 128 and 143 CCSF, where the barite separates were extremely low relative to the XRF.

5 Estimated $CaCO_3$ from GRA bulk density for Sites 848, 849, 850, and 851

We were unable to XRF scan Sites 848, 850, and 851 but can estimate $CaCO_3$ from the variation of wet bulk density of eastern tropical Pacific sediments (Mayer, 1991, Hagelberg et al, 1995; Lyle et al, 1995). We also did the GRA estimate for $CaCO_3$ for Site 849 to compare to the XRF scan estimate. The data are listed in **Tables SM-22 to SM-25**.

Before calculating the $CaCO_3$ the bulk density profile was decompacted (removing the effect of porosity loss by sediment burial) by subtracting the compaction calculation as formulated in Lyle et al (1995), where the compaction related density change D is as follows:

5    $D = 1.2(mbsf/1000) - 1.374(mbsf/1000)^2$ (4)

D is subtracted from the measured density at each depth to arrive at the decompacted density. All the decompacted density data from Sites 848, 849, 850, and 851 were calibrated with the discrete $CaCO_3$ data and the resulting scatter plot was fit with a power law estimate.:

10

$CaCO_3 \text{ (GRA estimate)} = 112.09 - 88.022(GRA_{decompact}{}^{-3.0513})$ (5)

Figure SM-4 compares the shipboard $CaCO_3$ measurements (blue dots) to the XRF scan $CaCO_3$ estimate (red line) and the GRA $CaCO_3$ estimate (brown line). We find that both the GRA and XRF give similar estimates for $CaCO_3$ %, but that the

15   GRA variability is somewhat attenuated, and the XRF scan calibration matches the shipboard CaCO3 % data slightly better.

6 Calculating Mass Accumulation Rates (MARs).

Mass accumulation rates are calculated from sedimentation rates and the dry bulk density of the sediment, multiplied by the fraction of the sediment composed of that component. They are sensitive to the quality of the sedimentation rate profile primarily, because the other measurements have relatively small error. The MAR equation is

20

$MAR_e = X_e * \rho_{dry} * S$ (6)

Where $\rho_{dry} * S$, the dry bulk density times the sedimentation rate, is the bulk MAR (the total solids rate of burial), X_e is the weight fraction of component "e" in the sediment, and MAR_e is the mass accumulation rate of component "e". MAR units are $g/cm^2/kyr$, if S is expressed as cm/kyr and ρ_{dry} is expressed in grams.

25

The chemical data were evenly spaced in depth but not in time. For this reason, we first interpolated the data to 1 or 2 kyr spaced data before smoothing. We also interpolated ρ_{dry} to the same temporal spacing as the chemical data. ρ_{dry} was calculated from a linear fit of GRA density data to the shipboard ρ_{dry} measurements. Because of slower sedimentation rates, Sites 848 and U1335 were interpolated to 2 kyr spacing, while the rest of the sites were interpolated to 1 kyr temporal

30   spacing.

After interpolation, the sediments were smoothed with a 20-point binomial smooth and resampled at 10 kyr intervals. The MAR data are posted in **Tables SM 26-32**. MARs are only calculated for calibrated XRF data and the GRA-estimated CaCO$_3$ data.

7 Evidence for Sediment focusing at Site U1337

Sediment focusing may inflate sedimentation at a drill site if there is net horizontal sediment transport to it and may cause incoherent changes at different drill sites if the current-deposited sediment adds significantly to the particles that rain from the ocean surface. Such focusing may have occurred at Site U1337.

Site U1337 has a higher than average sedimentation rate as compared to other sites at its latitude, 3.8°N, and has faster net sedimentation since 4400 ka than Site U1338, at 2.5°N (Figure 2 in main article). It is typical for sedimentation rates and MARs to decrease with latitude in the Pleistocene (Murray et al., 2000). Decreases in sedimentation rate and MAR with increasing latitude are typical for the Neogene as well (van Andel et al, 1975; Lyle, 2003). Thus we expected that sedimentation rates for a site near 4°N to be less than that for a site closer to the equator, and that it should be similar to other sites near 4°N. However, Site 574, at 4.2° N, 4568 m water depth, has a net accumulation of 40 m of sediment since the end of the Miocene as compared to 84 m over the same time period at Site U1337, which is only 100 m shallower and at 3.8°N. (Mayer et al, 1985; Pälike et al, 2010). More sediment accumulated since the Miocene at Site U1337 than at Site U1338 (69 m), located at 2.5°N and 100 m shallower than Site U1337.

Furthermore, there is clear evidence of erosion into the sediment column surrounding the plateau where U1337 sits (Figure SM-1b, Figure SM-5). The sediment at Site U1337 also has anomalously high MARs of opal and clay, as expected if a fine fraction is focused to Site U1337 (Lyle et al, 2014; Lovely et al., 2017). In Figure 6, the difference between the bulk MAR and the CaCO$_3$ MAR represents the deposition of clays and opal. Only Site U1337 has a bulk MAR profile that is significantly elevated relative to the CaCO$_3$ MAR and not coherent with it, showing excess deposition of fine fraction opal and clay. Despite the probable focusing, profiles of CaCO$_3$ % at Site U1337 resemble profiles from the other equatorial Pacific sites

References

Drury, A. J., John, C. M., and Shevenell, A. E.: Evaluating climatic response to external radiative forcing during the late Miocene to early Pliocene: New perspectives from eastern equatorial Pacific (IODP U1338) and North Atlantic (ODP982) locations, Paleoceanography, 31, 167-184, doi:10.1002/2015PA002881, 2016.

Drury, A. J., Westerhold, T., Frederichs, T., Tian, J., Wilkens, R., Channell, J. E. T., Evans, H., John, C. M., Lyle, M., and

Röhl, U.: Late Miocene climate and time scale reconciliation: Accurate orbital calibration from a deep-sea perspective, Earth and Planetary Science Letters, 475, 254-266, doi:10.1016/j.epsl.2017.07.038, 2017.

Drury, A. J., Lee, G. P., Gray, W. R., Lyle, M., Westerhold, T., Shevenell, A. E., and John, C. M.,: Deciphering the state of the late Miocene to early Pliocene equatorial Pacific, Paleoceanography and Paleoclimatology, 33, 246-263, doi:10.1002/2017PA003245, 2018.

Dymond, J., Corliss, J. B. and Stillinger, R.: Chemical composition and metal accumulation rates of metalliferous sediments from Sites 319, 320, and 321, DSDP Init Repts, 34, 575-588, 1976.

Lisiecki, L. E. and Raymo, M. E.: A Pliocene-Pleistocene stack of 57 globally distributed benthic $\delta^{18}O$ records, Paleoceanography, 20, PA1003, doi:10.1029/2004PA001071, 2005.

Lovely, M. R., Marcantonio, F., Lyle, M., Ibrahim, R., Hertzberg, J. E., and Schmidt, M. W.: Sediment redistribution and grainsize effects on 230Th-normalized mass accumulation rates and focusing factors in the Panama Basin, Earth and Planetary Science Letters, 480, 107-120, doi: 10.1016/j.epsl.2017.09.046, 2017.

Lyle, M., Dadey, K. and Farrell, J.: The Late Miocene (11-8 Ma) eastern Pacific carbonate crash: Evidence for reorganization of deep water circulation by the closure of the Panama Gateway. In: Proceedings of the Ocean Drilling Program, Scientific Results, 138, doi: 10.2973/odp.proc.sr.138.157.1995, 1995.

Lyle, M.: Neogene carbonate burial in the Pacific Ocean, Paleoceanography, 18, DOI 10.1029/2002PA000777, 2003.

Lyle, M., Olivarez Lyle, A., Gorgas, T., Holbourn, A., Westerhold, T., Hathorne, E. C., Kimoto, K. and Yamamoto, S.: Data report: raw and normalized elemental data along the U1338 splice from X-ray Fluorescence scanning, Proceedings of the Integrated Ocean Drilling Program, 320/321,doi: 10.2204/iodp.proc.320321.2010, 2012.

Lyle, M. and Backman, J.: Data Report: Calibration of XRF-estimated $CaCO_3$ along the Site U1338 splice, Proceedings of the Integrated Ocean Drilling Program, 320/321, doi: 10.2204/iodp.proc.320321.205.2013, 2013.

Lyle, M., Marcantonio, F., Moore, W. S., Murray, R. W., Huh, C.-A., Finney, B. P., Murray, D. W. and Mix, A. C.: Sediment size fractionation and sediment focusing in the equatorial Pacific: effect on ^{230}Th normalization and paleoflux measurements, Paleoceanography, 29, 747-763, doi:10.1002/2014PA002616, 2014.

Lyle, M., and Baldauf, J.: Biogenic sediment regimes in the Neogene equatorial Pacific, IODP Site U1338: Burial, production, and diatom community, Palaeogeography, Palaeoclimatology, Palaeoecology, 433, 106-128, doi:10.1016/j.palaeo.2015.04.001, 2015.

Ma, Z., Ravelo, A. C., Liu, Z., Zhou, L. and Paytan, A.: Export production fluctuations in the eastern equatorial Pacific during the Pliocene-Pleistocene: Reconstruction using barite accumulation rates, Paleoceanography, 30, doi:10.1002/2015PA002860, 2015.

Mayer, L. A., Theyer, F., Barron, J., Dunn, D. A., Handyside, T. Hills, S., Jarvis, I., Nigrini, C. A., Pisias, N., Pujos, A., Saito, T., Stout, P., Thomas, E., Weinrich, N. and Wilkens, R. H.: Initial Reports of the Deep Sea Drilling Program, 85, doi: 10.2973/dsdp.proc.85.1985, 1985.

Mayer, L. A.: Extraction of high-resolution carbonate data for palaeoclimate reconstruction, Nature, 352, 148-150, 1991.

Mayer, L. A., Pisias, N. G., Janecek, T., and Leg_138_Shipboard_Scientific_Party: Proceedings of the Ocean Drilling Program, Initial Reports, 138, Ocean Drilling Program, College Station TX, doi: 10.2973/odp.proc.ir.138.1992, 1992.

Mix, A. C., Pisias, N. G., Rugh, W., Wilson, J., Morey, A., and Hagelberg, T. K.: Benthic foraminifer stable isotope record from Site 849 (0-5 Ma): local and global climate change. . In: Proceedings of the Ocean Drilling Program, Scientific Results, 138, 371-412, 1995.

Murray, R. W., Knowlton, C., Leinen, M., Mix, A. and Polsky, C. H.: Export production and carbonate dissolution in the central equatorial Pacific Ocean over the past 1 Myr, Paleoceanography, 15, 570-592, 2000.

Olivarez Lyle, A. and Lyle, M.: Determination of biogenic opal in pelagic marine sediments: a simple method revisited. Proceedings of the Ocean Drilling Program, Initial Reports. 199, doi: 10.2973/odp.proc.ir.199.106.2002, 2002.

Pälike, H., Lyle, M., Nishi, H., Raffi, I., Gamage, K., Klaus, A., and the Expedition 320/321 Scientists, *Proc. IODP*, 320/321: Tokyo (Integrated Ocean Drilling Program Management International, Inc.). doi:10.2204/ iodp.proc.320321.2010, 2010b.

Ryan, W. B. F., Carbotte, S. M., Coplan, J. O., O'Hara, S., Melkonian, A., Arko, R., Weissel, R. A., Ferrini, V., Goodwillie, A., Nitsche, F., Bonczkowski, J. and Zemsky, R.: Global Multi-resolution Topography Synthesis, Geochemistry,

10

Geophysics, Geosystems, 10, Q03014, 2009. doi: 10.1029/2008GC002332

Shackford, J. K., Lyle, M., Wilkens, R., and Tian, J.: Data report: raw and normalized elemental data along the Site U1335, U1336, and U1337 splices from X-ray fluorescence scanning Proceedings of the Integrated Ocean Drilling Program, 320/321, doi:10.2204/iodp.proc.320321.216.2014, 2014.

Shackleton, N. J., Crowhurst, S., Hagelberg, T., Pisias, N. G. and Schneider, D. A.: A new late Neogene time scale: application to Leg 138 sites. Proceedings of the Ocean Drilling Program, Scientific Results, 138, 73-101, doi:10.2973/odp.proc.sr.138.106.1995, 1995.

Taylor, S. R. and McClennan, S. M.: The geochemical evolution of the continental crust, Reviews of Geophysics, 33, 241-265, 1995.

van Andel, Tj. H., Heath, G. R., and Moore, T. C. jr.: Cenozoic History and Paleoceanography of the central equatorial Pacific Ocean, GSA Memoir 143, Geological Society of America, 1975.

Wilkens, R. H., Dickens, G. R., Tian, J., Backman, J. and Expedition 320/321 Scientists: Data report: revised composite depth scales for Sites U1336, U1337, and U1338 Proceedings of the Integrated Ocean Drilling Program, doi: 10.2204/iodp.proc.320321.209.2013, 2013, 2013.

Wilkens, R., Westerhold, T., Drury, A. J., Lyle, M., Gorgas, T. and Tian, J.: Revisiting the Ceara Rise, equatorial Atlantic Ocean: isotope stratigraphy of ODP Leg 154 from 0 to 5 Ma, Climate of the Past, 13, 779-793, doi:10.5194/cp-13-779-2017, 2017.

Wilson, J. K.: Early Miocene carbonate dissolution in the eastern equatorial Pacific, Phd thesis, Oceanography, Texas A and M University, 155 pp., 2014.

Winckler, G., Anderson, R. F., Fleisher, M. Q., McGee, D., and Mahowald, N.: Covariant Glacial-Interglacial dust fluxes in the equatorial Pacific and Antarctica, Science, 320, 93-96, doi:10.1126/science.1150595, 2008.
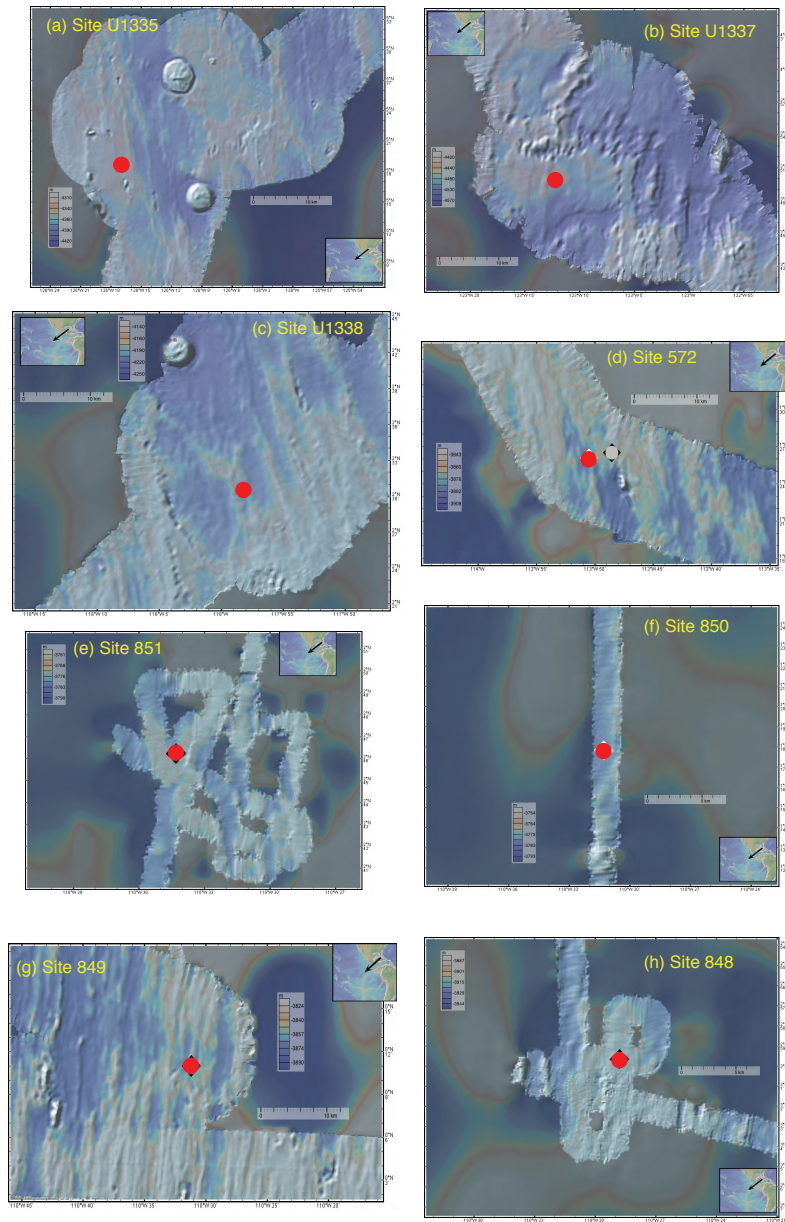
Figure SM-1. Bathymetric maps for equatorial Pacific scientific drill sites from DSDP, ODP, and IODP. Low resolution background bathymetry for all sites is from satellite gravity estimates of topography with a nominal 4 km grid, overlain by higher resolution ~100 m pixel multibeam data (Ryan et al, 2009). Multibeam data for Sites U1335, U1337, U1338, 572, and 849 were collected with on the AMAT-03 site survey for IODP Exp 320/321 on R/V Roger Revelle in 2006. Sites 851, 850, and 848 have only the 1989 seabeam surveys from R/V Thomas Washington taken during the site survey for ODP Leg 138 (VNTR-01). Red dots mark the drill sites. Large numbers of erosional channels were imaged to the north and east of Site U1337 (Fig SM-1b).
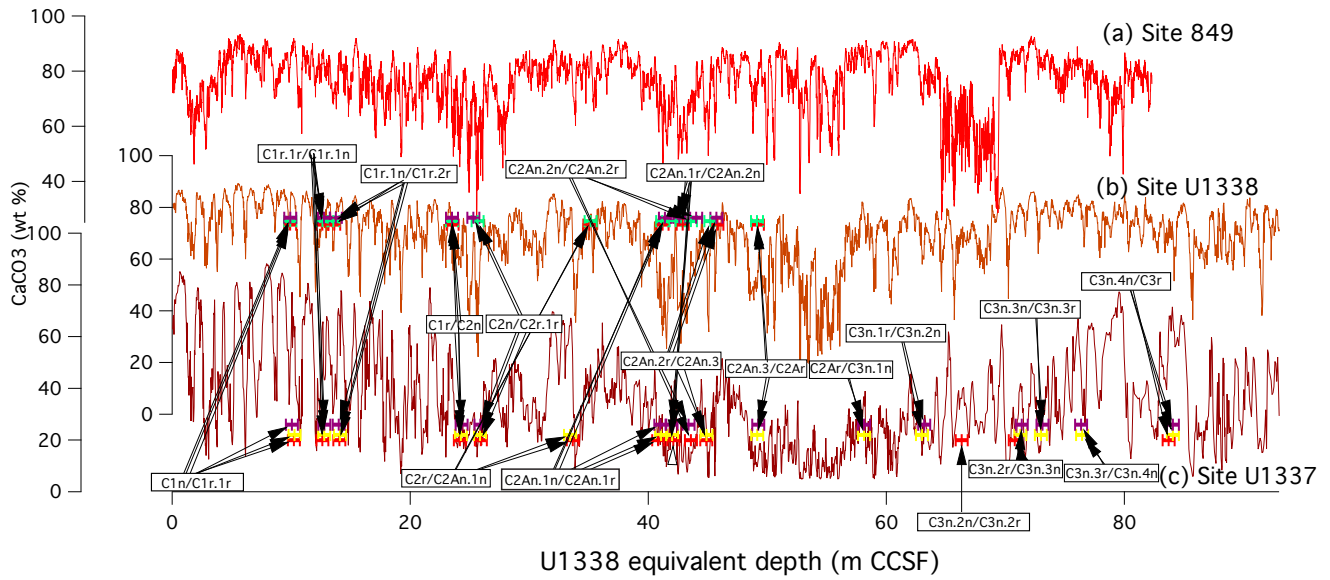
12

Figure SM-2. Three CaCO3% records from (a) Site 849, (b) Site U1338, and (c) Site U1337 shown on equivalent U1338 depth as calculated from site-to-site depth correlation. Paleomagnetic reversal stratigraphy is shown for Sites U1337 and U1338, which provided independent chronostratigraphic control. Reversals were recorded in multiple holes at each site and were used to infer the depth precision of each datum level.
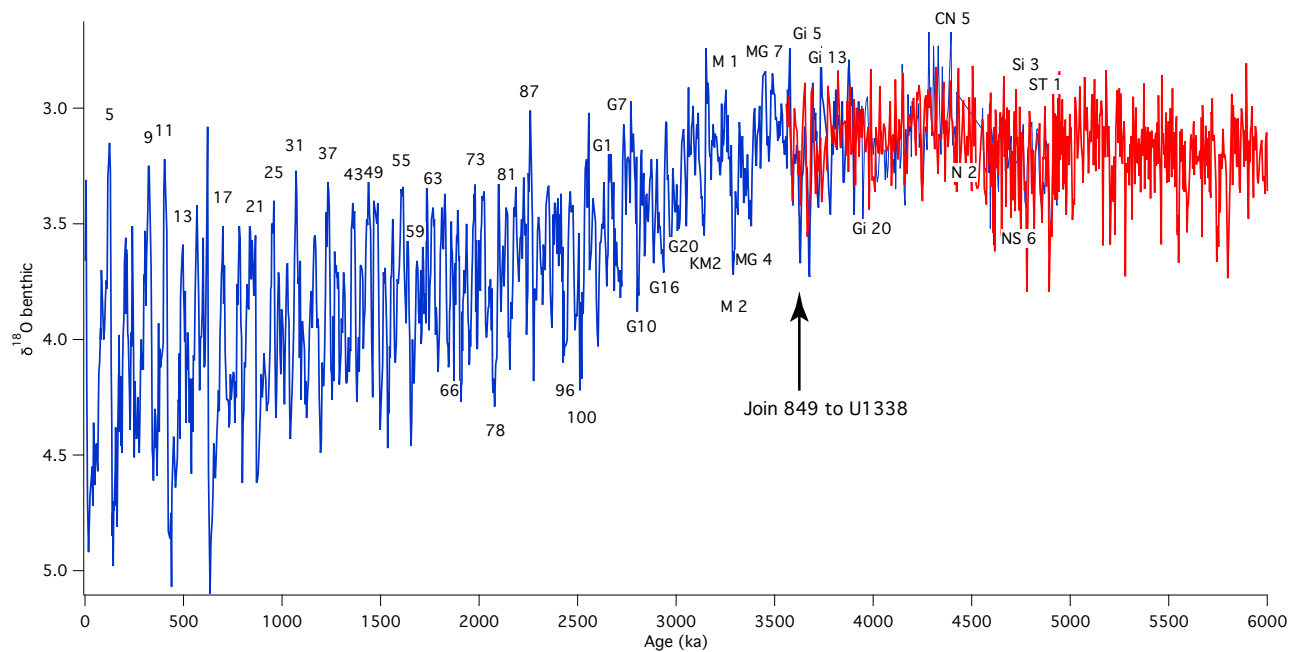
13

Figure SM-1: Site 849 benthic foraminiferal δ^{18}O (blue, data from Mix et al, 1995) tuned to the Ceara Rise isotope stack (Wilkens et al, 2017) plus the Site U1338 benthic foraminiferal δ^{18}O (red, Drury et al, 2018), that extends to 8180 ka. The combined age model was achieved by joining the 0-3626 ka section of Site 849 to Site U1338, marked by arrow.
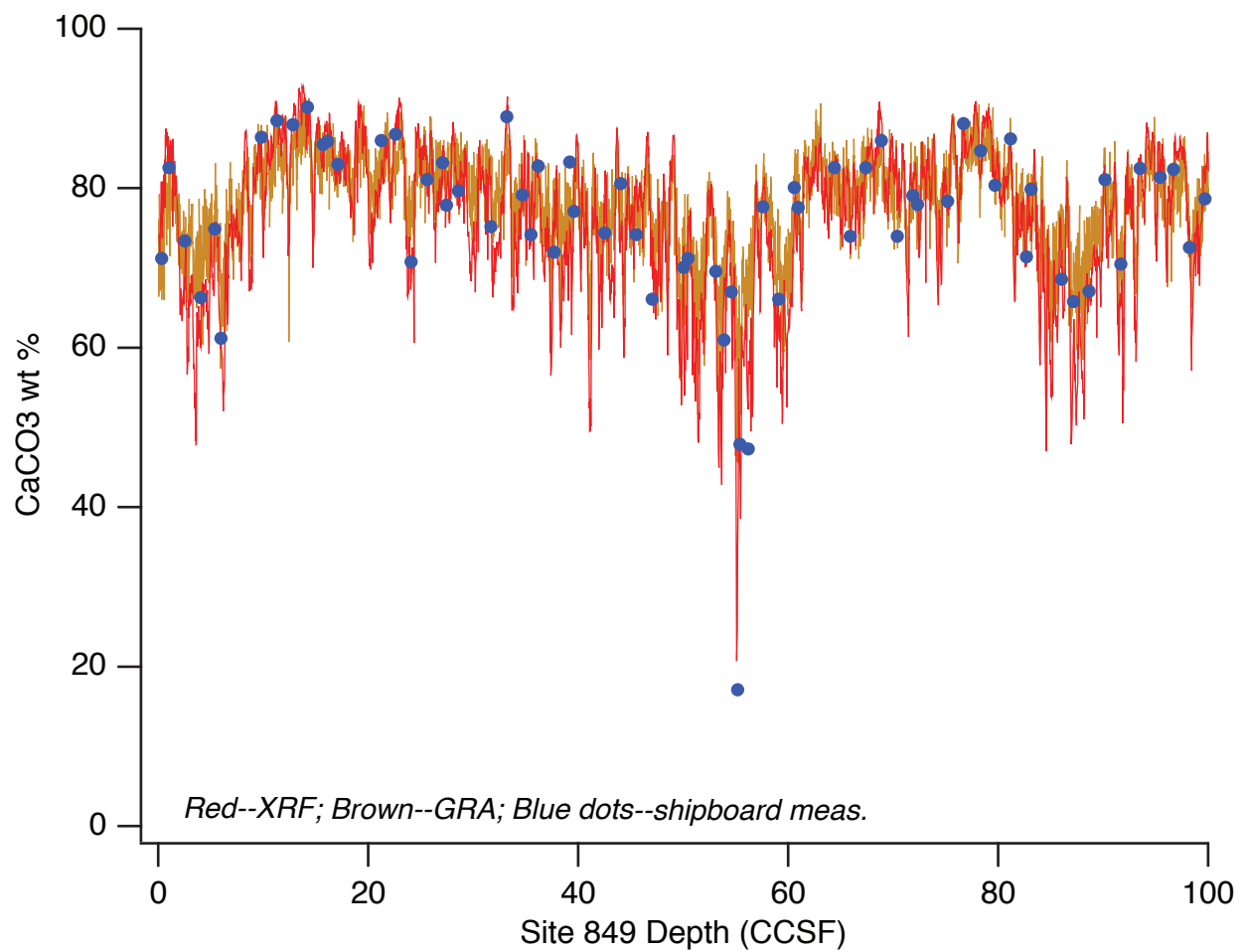
5

Figure SM-2: Site 849 CaCO₃ record, from shipboard measurements (blue dots), estimated by XRF Ca measurements (red line), and using the GRA density transform (brown line). The XRF and GRA estimates are similar, but XRF is slightly better to match the shipboard measurements.
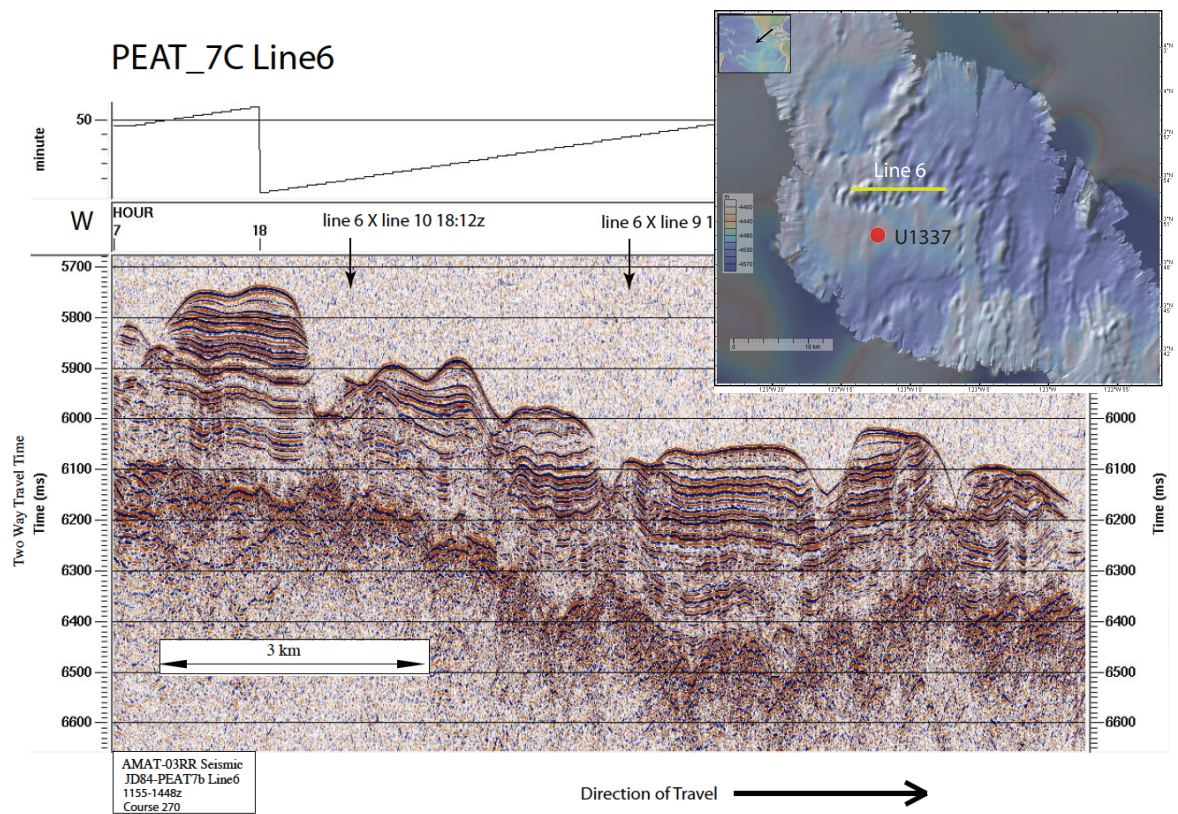
5

Figure SM-5: Evidence for sediment focusing at Site U1337. The bathymetry map (upper right) shows areas that appear to be erosional pits surrounding the plateau on which Site U1337 was sited. Line 6 from the site survey is one line that finds there has been erosion into the sediment column within the pits, truncating sedimentary horizons.

5